IC/94/49

INTERNATIONAL CENTRE FOR THEORETICAL PHYSICS

REALISTIC MODELLING OF OBSERVED SEISMIC MOTION IN COMPLEX SEDIMENTARY BASINS

D. Fäh

and

G.F. Panza

INTERNATIONAL ATOMIC ENERGY AGENCY

UNITED NATIONS EDUCATIONAL, SCIENTIFIC AND CULTURAL ORGANIZATION

MIRAMARE-TRIESTE

IC/94/49

International Atomic Energy Agency
and
United Nations Educational Scientific and Cultural Organization
INTERNATIONAL CENTRE FOR THEORETICAL PHYSICS

REALISTIC MODELLING OF OBSERVED SEISMIC MOTION IN COMPLEX SEDIMENTARY BASINS

D. Fäh
Istituto di Geodesia e Geofisica, Università degli Studi di Trieste, Trieste, Italy

and

G.F. Panza
International Centre for Theoretical Physics, Trieste, Italy
and
Istituto di Geodesia e Geofisica, Università degli Studi di Trieste, Trieste, Italy.

MIRAMARE - TRIESTE
March 1994

Abstract

Three applications of a numerical technique are illustrated to model realistically the seismic ground motion for complex two-dimensional structures. First we consider a sedimentary basin in the Friuli region, and we model strong motion records from an aftershock of the 1976 earthquake. Then we simulate the ground motion caused in Rome by the 1915, Fucino (Italy) earthquake, and we compare our modelling with the damage distribution observed in the town. Finally we deal with the interpretation of ground motion recorded in Mexico City, as a consequence of earthquakes in the Mexican subduction zone. The synthetic signals explain the major characteristics (relative amplitudes, spectral amplification, frequency content) of the considered seismograms, and the space distribution of the available macroseismic data. For the sedimentary basin in the Friuli area, parametric studies demonstrate the relevant sensitivity of the computed ground motion to small changes in the subsurface topography of the sedimentary basin, and in the velocity and quality factor of the sediments. The total energy of ground motion, determined from our numerical simulation in Rome, is in very good agreement with the distribution of damage observed during the Fucino earthquake. For epicentral distances in the range 50km-100km, the source location and not only the local soil conditions control the local effects. For Mexico City, the observed ground motion can be explained as resonance effects and as excitation of local surface waves, and the theoretical and the observed maximum spectral amplifications are very similar. In general, our numerical simulations permit the estimate of the maximum and average spectral amplification for specific sites, i.e. are a very powerful tool for accurate micro-zonation.

Introduction

The presence of unconsolidated sediments with irregular geotechnical characteristics makes the sedimentary basins the zones which are most vulnerable to earthquakes. In fact, when the shear-wave velocity at the surface is low, quite large amplifications of the ground motion are observed, and localized amplification of the signals are often related to lateral irregularities in the subsurface topography (e.g. Jackson, 1971). Even smooth variations of the near-surface structure can cause large differential motion, and in relatively close points it is possible to observe signals with significantly different amplitude and duration.

It is well-known that incident plane waves are amplified when the seismic wave travels through an interface from a medium with high rigidity, into a medium with low rigidity. For vertically incident waves, the frequencies of the mechanical resonance which can occur in sedimentary basins, are given by $f_n=(2n+1)\beta/4h$, where β is the shear wave velocity in the basin and h is its thickness (Haskell, 1960; 1962). An irregular interface between bedrock and sediments can cause the focusing of waves (e.g. Aki and Larner, 1970; Boore et. al., 1971; Sánchez-Sesma et al., 1988), and can excite local surface waves (e.g. Trifunac, 1971; Bard and Bouchon, 1980a; 1980b). These local surface waves can be excited not only by body waves but also by the incidence of surface waves (Drake, 1980). Bard and Bouchon (1985) demonstrated that the occurrence of local surface waves is determined primarily by the depth of the basin and by the contrast between the shear-wave velocity of the basin and that of the bedrock. When the wavelength of the incident wave is comparable with the depth of the basin, the local surface waves can have larger amplitudes than the direct signal, and, if the contrast in the elastic parameters between the sediments and the underlying bedrock is high, they can be reflected at the edges of the basin, causing a long duration of the ground motion in the basin. This behavior does not change if a vertical stratification of the sediments, with a large vertical velocity gradient, is considered (Bard and Gariel, 1986).

For preparedness purposes, it is crucial to estimate the seismic ground motion, before an earthquake occurs, and to include these results in the assessment of seismic hazard or in (micro)-zonation studies. A powerful tool to estimate the amplification effects in complex structures are numerical simulations. One major problem which is encountered when doing such simulations is the large number of parameters which have to be specified as input. The choice of these parameters should be based on all available seismological, geological and geotechnical information for the area under consideration. At a specific site, the numerical simulation can predict the seismic response only if the properties of the seismic source and the mechanical (density, velocity, damping, etc.) and geometrical (such as thickness) parameters of the path from the source are reasonably well-known. In general this is not the case, and parametric studies are necessary to quantify the variability of the expected ground motion. Such simulations, whenever possible must be compared with observed ground motion.

The method we use for the modelling of the wave propagation in two-dimensional complex media, is the hybrid technique, which combines modal summation (Panza, 1985; Florsch et al., 1991) and the finite difference technique (Korn and Stöckl, 1982; Virieux, 1986), described by Fäh (1992), Fäh et al. (1993a; 1993b), and Fäh et al. (1994). The propagation of waves from the source to the sedimentary basin is treated with the mode summation method, applied to plane layered, anelastic structures which represent the average crustal properties along the source-basin path. In our modelling, this structure is used as the reference, bedrock model. The wavefield computed for this bedrock model is used as incident wavefield for the explicit finite difference schemes, which are used to simulate the propagation of seismic waves in the two-dimensional, anelastic model of the sedimentary basin. This hybrid method allows us to take into account the source and propagation effects, including local soil conditions, even when dealing with path lengths of a few hundred kilometers.

In the following, we illustrate a comparison between numerical simulations, and observed strong ground motion or the space distribution of the available macroseismic data. We will focus on the different effects of the source, the path and the local soil conditions. Special emphasis is given to understand the different features of ground motion in sedimentary basins, and the application of numerical simulations for seismic zonation. The three applications include sites close to the

source (a sedimentary basin near to the epicenter of the September 11, 1976, Friuli aftershock at $16^h35^m04^s$), at an intermediate distance (Rome, about 80 km from the epicenter of the January 13, 1915, Fucino earthquake), and sites that are far from the source (Mexico City, about 400 km from the epicenter of the September 19, 1985, Michoacan earthquake).

The sedimentary basins in the Friuli area

The September 11, 1976 Friuli aftershock ($16^h35^m04^s$) has been recorded by a few accelerographic stations (CNEN-ENEL, 1977). Records from one of the nearest stations - the three-component records at station Buia (Figure 1)- are considered and compared with the theoretical computations. We focus on the variability of ground motion within the sedimentary basin, and on the sensitivity of the computed ground motion to small changes in the subsurface topography of the sedimentary basin, and in the velocity and quality factor of the sediments.

The bedrock model, describing the average mechanical properties of the path from the epicenter to the sedimentary basin, has been proposed by Fäh et al. (1993a), and its uppermost layers are shown in Figure 2. The source-depth used in the numerical modelling is 7.1 km, the angle between the strike of the fault and the epicenter-station line 19°, the dip 28°, the rake 115°, and the source duration is 0.6 s (Florsch et al., 1991).

The area where the station of Buia is located is characterized by terrigenous sediments (Flysch), widely outcropping at Monte Buia (Figure 1), which are covered locally by a thin quaternary layer, forming a sedimentary basin, and which overlap a carbonatic mesozoic sequence. The thickness of the quaternary sediments is well-known (Giorgetti and Stefanini, 1989) and locally can reach 100 m. The average model for the sedimentary basin is represented by the cross-section B, while the part of the basin with a thick sedimentary cover is well represented by the cross-section C, both shown in Figure 2.

The accelerograms obtained in correspondence of the cross-section B, with the shear-wave velocity of the unconsolidated sediments equal to 0.6 km/s and the quality factor Q_β equal to 20, are shown in Figure 3. At sites with a thick layer of low-velocity material near to the surface, the peak acceleration of the radial component is up to

two times larger than the vertical component, while, due to the source radiation pattern, the transverse component is of the same size of the radial component.

The heterogeneity, with size comparable to the wavelength of the incident wavefield, causes significant spatial variations in the ground motion (Figure 3). There are three major effects which are caused by the presence of the sedimentary cover: (1) the excitation of surface waves at the edge of the sedimentary basin, (2) the resonance in parts of the basin due to the subsurface topography of the bedrock, and (3) the excitation of very dispersed local surface waves, with peak energy at about 2 Hz, within the sedimentary basin for epicentral distances larger than 14 km.

Multiple reflections of SH-waves can generate local surface waves, (phase L_1) - forming the coda of the signals (Figure 3) - which are excited as soon as the fundamental Haskell's frequency of resonance (Haskell, 1960; 1962) for the sedimentary basin is reached. These local surface waves can be reflected inside the basin at places where the sediments become thin. One example is given by the phase L_{11} in Figure 3, which corresponds to the reflected local surface wave L_1. Also for P-SV-waves, a dipping layer at the edge of a sedimentary basin gives rise to multiple reflections of body waves and the excitation of local surface waves (phase R_2 in Figure 3), which are characterized by larger amplitudes on the radial than on the vertical component of motion, and can be the dominant part of the wavefield at the edge of the sedimentary basin. The reflections of the local Rayleigh waves inside the sedimentary basin (R_{22} in Figure 3) do not appear as clear as in the case of Love waves, since their amplitudes are small in comparison with the amplitudes of the primary waves.

Resonance occurs in those parts of the basins where the interface between the bedrock and the sediments is smoothly varrying, and originates from the superposition of forward propagating local surface waves with their reflections, within sub-basins of the sedimentary cover. Examples are seen for the two sub-basins in cross-section B, especially at 9.8 km and at 11.8 km from the source (Figure 3). The resonance is stronger for SH- than for P-SV-waves, and in general can give rise to very large duration and amplitude, as can be seen from the signal computed at 11.8 km from the source.

The excitation of strongly dispersed local surface waves by subsurface lateral heterogeneities can be observed in correspondence of the cross-section B at epicentral distances larger than 14 km, both for SH- and P-SV-waves.

The synthetic accelerograms, obtained from the numerical modelling, can be used to compute some ground motion related quantities. These quantities are (1) the peak ground acceleration PGA and (2) the so-called total energy of ground motion, W, given by:

$$W = \lim_{t \to \infty} \int_0^t [\ddot{x}(\tau)]^2 \, d\tau \quad ,$$

where x(t) is the time series describing the ground displacement. To discuss the site effects with respect to the bedrock model it is convenient to consider the quantities PGA(2D), and W(2D), i.e. PGA and W obtained from the accelerograms computed for the two-dimensional model, and PGA(bedrock) and W(bedrock), i.e. PGA and W obtained from the accelerograms computed for the model representing the average properties of the source-basin path. The ground motion computed for the different sites in the two-dimensional model is normalized with respect to the ground motion obtained for the same source-receiver distance considering the bedrock model.

The spatial distribution of the values of the relative PGA (PGA(2D)/PGA(bedrock)) and relative W (W(2D)/W(bedrock)) for the transverse component of motion, and for different shear-wave velocities and quality factors of the unconsolidated sediments are shown in Figure 4. The relative PGA increases only slightly when the shear-wave velocity of the sediments is reduced, whereas the relative W is very sensitive to small changes in the shear-wave velocity of the sediments. A low shear-wave velocity induces the largest amplitudes and dispersion of the local surface waves. These effects give the dominant contribution to the relative W at sites where resonance effects and excitation of local surface waves are important (for example at 11.8 km from the source). The relative PGA and W have been computed for three different quality factors Q_β of the sediments, by keeping the shear-wave velocity fixed at 0.6 km/s (right part of Figure 4). The attenuation of waves increases with decreasing quality factor. This causes the reduction of the duration of the signals at sites where resonance effects and excitation of local surface waves are important phenomena. The smaller the quality factor of the unconsolidated

sediments, the shorter is the duration of the resonance, and the smaller the propagation distance of the local surface waves. Consequently, low quality factors strongly reduce the relative W.

In Figure 5, we compare the synthetic signals computed for the two cross-sections B and C, shown in Figure 1, with the accelerograms recorded at station Buia. In correspondence of the recording station, which is at 15 km from the source, the thickness of the sedimentary cover is the same in the two cross-sections.

For the transverse component of motion, the local surface waves have amplitudes that are too large in comparison with the observation. In the choice of the geometry of the bedrock-sediment interface, we have restricted ourselves to that given by Giorgetti and Stefanini (1989). However, to reproduce the observed transverse component, the heterogeneity inside the sedimentary basins, responsible for the excitation of these local surface waves, would have to be different. The considered heterogeneity is either too close to station Buia or the bedrock-sediment interfaces are too close to the free surface. In the radial component the excitation of local surface waves is not very clear. When dealing with P-SV-waves, there are two sources of local surface waves: the edge of the sedimentary basin and the places where the bedrock-sediment interface approaches the free surface. From the signals computed for the two cross-sections, it can be concluded that the closer the sediment-bedrock interface is to the free surface, the greater are the amplitudes of the local Rayleigh waves. On the other hand, this lateral heterogeneity can cause the reflection of most of the local Rayleigh waves, generated at the sedimentary basins edge which is closer to the seismic source.

The comparison of the synthetic signals with the observed radial component shows good agreement between the observation and the signal obtained for cross-section C. Due to the small amplitudes of the coda in the observation, it can be concluded that the local surface waves have travelled through the deeper parts of the sedimentary basin, and that the lateral heterogeneity within the basin has reflected a relevant part the local surface waves, which is excited at the edge of the basin. To reproduce the observed signal, the lateral heterogeneity within the basin cannot be strong; a strong heterogeneity, in fact, would excite large-amplitude local surface waves inside the basin, and these are not observed experimentally.

The vertical component of the observed ground motion, especially at low-frequency (below 4 Hz), is quite similar to the synthetic signals, which do not change significantly from one cross-section to the other. The relatively small sensitivity of the vertical component of motion to the lateral variation of sedimentary basins has been observed also at different sites in Mexico City, and the results illustrated in this paper suggest to consider this fact a quite general property of sedimentary basin. The high-frequency component, not observed experimentally, but present in the synthetic signals for models B and C, is due to the resonance effects in the shallow part of the sedimentary cover. This difference between the computed and the observed signals indicates once again that, in the modelling, either the shallow parts of the sedimentary cover are too close to the observation point, or the bedrock-sediment interfaces are too close to the free surface.

The Rome area and the 1915 Fucino earthquake

The area of Rome, considered here, is characterized by several sedimentary basins of considerable thickness, which, in some parts, are covered by volcanic rocks. The area is very vulnerable to earthquakes, as indicated, for example, by the well documented damage distribution caused by the January 13, 1915, Fucino (Italy) earthquake (M_L=6.8) (Figure 6). Since no strong motion records are available for this event, we have applied the hybrid technique to explain the observed damage distribution (Fäh et al., 1993b). The source parameters, the bedrock model, describing the path from the source to Rome, and the two-dimensional model for the area of Rome are described in Fäh et al. (1993b).

To demonstrate that not only the local soil conditions are important to explain a local distribution of damage, but that there are also important regional effects due to the source location, we compare the results of two sets of computations, made by changing only the distance of the seismic source from the city of Rome (Figure 7). The epicenter of the Fucino event is about 85 km east of Rome, and the other hypothetical source, source 2 in Figure 7, is located at a distance of about 65 km, in the same direction.

The synthetic accelerograms are used to compute the total energy, W(2D), and the relative total energy, W(2D)/W(bedrock), of ground motion. The results for the

transverse component of motion, corresponding to the two source positions are shown in Figure 8. They are compared with the histogram of the damage distribution, which has been constructed by projecting each observation of damage, shown in Figure 6, on the cross-section used in the numerical modelling (Fäh et al., 1993b). Only those points of the distribution have been used which are located in an area where the geometry of the structure does not differ too much from the geometry of the two-dimensional cross section. This area is delimited in Figure 6 by the two dotted lines. Since neither the type of buildings nor the density of the urbanization can be known with great detail, the histogram shown in Figure 8 should be interpreted only in a qualitative manner.

The total energy, W, and the relative W, computed for the Fucino event are quite well correlated with the damage distribution, as is shown in Figure 8 (Fäh et al., 1993b). There are four relative peaks: two at the edges of the Tiber basin, one within the alluvial valley of the Aniene river, and a broad peak where the Sicilian low-velocity zone gets close to the surface. The largest values are observed at the margins of the Tiber bed. There the signals have the largest amplitudes and duration, due to the low impedance of the alluvial sediments, the excitation of local surface waves, and resonance effects. Minimum values can be observed for sites placed above the volcanic layer overlying the Paleotiber basin, which acts as a shield, and reflects part of the incoming energy: the thicker the volcanic layer, the smaller are the W values observed at the surface.

The results obtained considering source 2 are quite different. W, and relative W are similar in the area of the Paleotiber basin, whereas in the other areas the values obtained considering source 2 are considerably smaller, and the two peaks at the margin of the Tiber basin are significantly reduced. A comparison of W, determined from the two numerical experiments, shows that the total energy associated with the Fucino event is significantly larger than the one carried by source 2, even if the former event is 20 km farther from Rome than the latter.

These differences can be explained by the attenuation of PGA and W with distance. The example concerning the transverse component of motion, computed for the bedrock model, is shown in Figure 9. The PGA and W are not monotonically decreasing with distance. This behavior is due to the fact that for epicentral distances less than 50 km the PGA and W are essentially controlled by the crustal Sg phase, while at greater distances they are increasing owing to the contribution of several S-

wave phases reflected mostly at the Moho (Suhadolc and Chiaruttini, 1985), which gradually become a part of the Lg waves and further increase PGA and W.

At distances of the order of 80 km (average distance of the Paleotiber from the Fucino event) and 60 km (average distance of the Paleotiber from the hypothetical source), the W values are about the same. This explains the similar values of W in the area of the Paleotiber (Figure 8) computed considering the two events. Similarly, it is possible to explain the values of W observed at distances in the range 61 km-67 km from source 2 (Figure 8), which are smaller than the ones corresponding to the Fucino event in the epicentral distance range 81 km-87 km. Finally from Figure 9, it is evident that, when dealing with earthquakes occurring in the Apennines, for epicentral distances between 50 and 100 km, the largest damage can be expected from an event as far as 90 km from Rome.

The Fourier-spectrum of the signal computed at 85km from the source, corresponding to the epicentral distance of the margin of the Tiber basin from the Fucino event, is quite large for frequencies below 2.5 Hz if compared with the spectrum of the signal obtained at 65 km from the source, which corresponds to the epicentral distance of the margin of the Tiber from source 2 (Figure 10). As we will see later, for frequencies below 2.5 Hz strong amplifications occur at the margins of the Tiber basin. Since the incident wavefield computed for source 2 contains relatively small energy at frequencies below 2.5Hz, resonance effects and excitation of local surface waves are not the dominant phenomena, and this justifies the absence of the peak at the margin of the Tiber basin in W computed for source 2. Thus, for epicentral distances in the range 50km-100km, the source location and not only the local soil conditions control the local site effects.

All the quantities used to measure strong ground motion like the maximum amplitude, the duration and the Fourier spectrum provide only a very limited description of the ground motion and certainly do not quantify its damage producing potential. A better quantity is the spectral acceleration Sa of the earthquake ground motion. A representation of the local soil effects is given by the spectral amplification Sa(2D)/Sa(bedrock) computed from the spectral accelerations obtained for the two-dimensional and the bedrock models. This procedure allows us to identify the frequency bands and sites at which amplification and attenuation effects occur. For SH-waves, the spectral amplification for zero damping are shown in Figure 11 for the two simulated events, as a function of frequency and of the spatial location along the

section. The darker an area, the stronger the amplifications due to the two-dimensional effects. The greatest amplification is observed for the Fucino event at the western edge of the sedimentary basin of the Tiber river (about 87 km from the source), for frequencies around 2 Hz. The maximum amplification is of the order of 5-6, and it is due to the combination of resonance effects and the excitation of local surface waves. This amplification effect is responsible for the relative peak in the total energy W at the margin of the Tiber basin (Figure 8).

The global distribution of the shaded areas can be related to the geometry of the structural model. The results are similar for the Fucino event and for source 2, except at the margins of the Tiber basin. An amplification over almost the entire frequency band is observed outside the Paleotiber basin (82-87 km from the source for the Fucino event, 62-67 km from source 2). Some amplification occurs in the Aniene basin, for frequencies above 2 Hz. For frequencies above 0.8 Hz, in the Paleotiber basin, the volcanic layer acts as a shield reflecting part of the incoming energy, and the values of the spectral amplification are smaller than 1. The underlying sedimentary complex (Sicilian) causes spectral amplification of the order of 2-3, due to resonances, which are most pronounced at frequencies around 0.4 Hz, where the fundamental resonance of this low-velocity zone is excited. In this part of the Paleotiber, in the frequency band 1.5-2.0 Hz, there is also evidence for the excitation of some higher modes of resonance. At distances of the order of 82-83 km from the Fucino event, and 62-63 km from source 2, between the Paleotiber and the Tiber basins, where the wave guide and overlying volcanic cover are thinning, focusing of seismic energy occurs and most of the trapped energy reaches the surface. This leads to amplifications, of the order of 2, over almost the entire frequency band considered. Therefore, the presence of a near-surface layer of rigid material is not sufficient to classify a site as a "hard-rock site". Reliable determinations of local soil effects, in addition to the knowledge of the frequency content and direction of the incoming signal, require the knowledge of both the thickness of the surficial layer and of the deeper parts of the structure, down to the real bedrock. This is especially important in volcanic areas, where pyroclastic material often covers alluvial basins.

Mexico City

Mexico City is an area of particular interest since extensive damage occurred in the lake-bed zone during the Michoacan earthquake of September 19, 1985. This can be attributed to the geotechnical and geometrical characteristics of the unconsolidated sediments in this zone. From the geotechnical point of view, the valley of Mexico City can be divided into the hill zone, the transition zone, and the lake-bed zone (Figure 12). The hill zone is formed by alluvial and glacial deposits, and by lava flows. The transition zone is mainly composed of sandy and silty layers of alluvial origin. The surficial layers in the lake-bed zone consist mainly of clays. These deposits are poorly consolidated, with high water content and very low rigidity. The thickness of this surficial layer varies between 10 m and 70 m, and increases regularly towards the east (Suarez et al., 1987). The clay layer is overlying the so-called "deep sediments" found below 10-70 m. These deeper deposits reach depths of the order of 700 m, with an uncertainty which may be as large as a few hundred meters (e.g. Bard et al., 1988). There are three outcrops of the basement: at Chapultepec, Peñon, and Cerro de la Estrella (Figure 12). In the last years, a strong motion network has been operating in the valley of Mexico City (e.g. Mena et al., 1986; Espinosa et al., 1990), and the positions of the stations used in this study are shown in Figure 12.

Today's research, to understand the extensive damage caused by the 1985 earthquake and the recorded ground motion in Mexico City, has shown the importance to consider source and propagation effects, including local soil conditions. This is dealt explicitly in the recent work by Fäh et al. (1994) in which the hybrid technique has been applied to study the ground motion in Mexico City. The model used by Fäh et al. (1994) explains the observed difference in amplitudes for receivers located inside and outside the lake bed zone. The ratio between the computed, horizontal peak ground displacements inside and outside the lake-bed zone reaches values ranging from 5 to 7, and about the same ratio is obtained for the observed ground motion. The validity of the modelling is further confirmed by the fact that the spectral ratios obtained for the horizontal components of the synthetic seismograms are very similar to comparable spectral ratios obtained from observations.

The structural model used in the numerical simulations for the 1985 Michoacan event, and a detailed parametric study of the effects of different soil

properties in Mexico City is given in Fäh et al. (1994). The flat-layered structure in Table 1 describes the path from the seismic source to the valley of Mexico City (Campillo et al., 1989). The structural model is rather simple, in agreement with the resolving power of the available data. The depth of the Moho is about 45 km, and the upper five kilometers are composed of low-velocity material. The two-dimensional structure for the Mexico City valley, modelling the Chapultepec-Peñon cross-section (solid line in Figure 12), is shown in Figure 13.

As in Fäh et al. (1994), to keep the source model as simple as possible and to avoid any, a priori, enhancement of resonance effects at the longer periods (above 2s), we consider first a constant, frequency independent, seismic moment rate spectrum. The focal mechanism is the one proposed by Campillo et al. (1989), based on the results of Houston and Kanamori (1986) and Riedesel et al. (1986). The distance from the source to the valley of Mexico City is 400 km, the angle between the strike of the fault and the epicenter-station line is 220°, the source depth is 10 km, the dip 15°, and the rake is 76°.

The use of an instantaneous time-function gives rise to synthetic signals that contain too much energy at high frequency (above 0.6Hz), and we can remove this drawback applying the ω^2 scaling law for the seismic moment rate spectrum, proposed by Kanamori et al. (1993) for the events occuring in the Mexican subduction zone:

$$\widehat{M} = M_0 \omega_c^2 \, (\omega^2 + \omega_c^2)^{-1} \qquad (1)$$

where $\widehat{M}$ is the seismic moment rate spectrum, M_0 is the seismic moment, and ω_c is the corner angular frequency. Following Kanamori et al. (1993), ω_c=0.196 s^{-1} and M_0=0.5 10^{21} N m. With these values we obtain a very good reproduction of the shape of the observed signals, over the entire frequency spectrum, but the absolute observed accelerations are underestimated by a factor ranging from 6 to 3. This last discrepancy can be reconciled considering the errors affecting the estimates of ω_c and M_0, and taking into account the subsequent rupture episodes of the Michoacan event, mainly the one occurring about 26s after the origin time. This kind of data fitting is, however, outside the purpose of the present paper, since it is unrelevant for the computation of the spectral amplification, and will be the subject of future investigations.

Spectral amplification at the site of interest computed with respect to a reference site gives a very good representation for micro-zoning purpose, especially from the engineering point of view (Fäh and Suhadolc, 1994). We compute the spectral amplification, i.e. the relative spectral accelerations Sa(2D)/Sa(Ref) and the relative spectral velocities Sv(2D)/Sv(Ref), for zero damping and 5% damping. Sa(2D) is the spectral acceleration and Sv(2D) is the spectral velocity obtained for the receivers in the two-dimensional structural model shown in Figure 13. Sa(Ref) and Sv(Ref) are the values obtained for the reference station shown in Figure 13. For all the receivers, we have computed the relative spectral accelerations and velocities for one hundred frequencies of the oscillator in the range 0.1-1.0 Hz. From these values we then computed the maximum spectral amplification (MSA) for the entire sedimentary basin. The MSA obtained from our numerical simulations are shown in Figure 14. The results for the relative spectral accelerations and the relative spectral velocities are similar, due to the approximate relation existing between them:

$$Sa(\omega)=\omega \cdot Sv(\omega),$$ where ω is the angular frequency of the oscillator.

In the following, we will, therefore, limit ourselves to the relative spectral velocities, which we will call spectral amplification.

In two-dimensional modelling, the SH-waves (transverse component of motion) and P-SV-waves (radial component of motion) are two independent wave fields. The direction of propagation of the local surface waves in the sedimentary basin is therefore well correlated with the source-receiver direction. In Mexico City, the local surface waves are excited at different locations of the interface between the bedrock and the sediments, and the direction of propagation of the local surface waves in the lake-bed zone does not correspond anymore to the source-receiver direction (F.J. Sánchez-Sesma, personal communication). Therefore, to justify the comparison between the observed ground motion and the synthetic signals, we have to compute the spectral amplification for the complete horizontal ground motion. For this purpose, we have applied the horizontal ground motion to an oscillator with two-degrees of freedom. The results for the synthetic signals are also given in Figure 14. Due to the larger amplitudes of the SH-waves, the MSA obtained for the horizontal ground motion are very similar to the result obtained for the transverse component. The maximum peaks in the MSA in Figure 14 can be attributed to sites where a strong interaction between the deep sediments and the surficial clay layer occurs. At such sites, the resonance frequencies of the two layers are almost the same.

The MSA obtained from the numerical simulation is rather independent from the shape of the seismic moment rate spectrum, as can be seen in Figure 15, where the results obtained with the seismic moment rate spectrum proposed by Kanamori et al. (1993) are compared with the results obtained for a frequency-independent spectrum.

The seismograms observed during the 1985 Michoacan earthquake, have been convolved with a high-pass Ormsby filter (Mena et al., 1986), and this filtering allows us an estimate of MSA only for frequencies above 0.1-0.2 Hz. The MSA, determined from the stations SC and CD using TY as reference, and shown in Figure 16, reaches lower values than those computed theoretically, as can be seen from a comparison with Figure 15. This is due to the fact that the site of station TY is not a hard rock site (e.g. Ordaz and Faccioli, 1993). Therefore, if any station in the transition zone or hill zone is taken as reference station, the MSA must be smaller than or equal to the theoretical values. For the Michoacan earthquake we have usable signals only from the stations CD, SC and TY, but we can test our theoretical results using observations from other events, such as the April 25, 1989 earthquake, since with our method, it is relatively easy to estimate the ground motion in a two-dimensional sedimentary basin if the ground motion is known at a reference point outside this basin (e.g. Luzon et al., 1994).

The epicenter of the 1989 event is located in the Guerrero gap, i.e. south of the epicenter of the 1985 Michoacan earthquake. Therefore, to justify a comparison between the numerical results based on the modelling of the 1985 event and the ground motion observed during the 1989 earthquake, we first have to compare the results obtained from the analysis of the records of the 1985 and 1989 earthquakes. The spectral amplification is shown in Figure 17, for station CD with respect to TY, both for the 1985 and for the 1989 earthquake. For the two events, the amplification effects at station CD occur in about the same frequency ranges. There is some difference in the maximum value, which is larger for the 1985 earthquake. The strong peaks in the spectral amplification observed at the station CD, during the 1985 earthquake, can be due to the fact that a relevant amount of energy of the incident wave field is present in the frequency band close to the resonance frequency of the clay layer at the site, and, therefore, local surface waves and resonance effects may dominate the horizontal components of motion. The two peaks in the MSA can be

attributed to the deep sediments (peak at about 0.8 Hz) and the surficial clay layer (peak at about 0.25 Hz) (Fäh et al., 1994).

The observed MSA for the 1989 earthquake is shown in Figure 18. The MSA is determined for all the stations shown in Figure 12 using as reference station TY and station 78. The MSA obtained with the reference station TY (Figure 18a and 18c) has once again lower values than those computed theoretically (shown in Figure 15). This is due to the fact, mentioned before, that the station TY is not located on hard bedrock. The MSA obtained with the reference station 78 (Figure 18b and 18d), on the other hand, is very similar to the theoretical curves shown in Figure 15. The peaks, for zero damping of the oscillator, occur when the energy of the incident wave field is relevant in the frequency band close to the resonance frequency of the clay layer at the site of interest. This happens in different sites within the lake-bed zone, and therefore each peak in the MSA (Figure 18b) is obtained from a different receiver. The maximum values obtained theoretically and from the observations are about the same, and the greater complexity in the observed MSA for zero damping, with respect to the theoretical one, which has only two peaks around 0.27 Hz and 0.47 Hz (Fig. 15a and 15b), is not surprising since our numerical model is restricted to one cross section. Therefore, since in our model the maximum clay thickness is 65 m, the MSA shown in Figure 15 is valid only for sites in the lake-bed zone that are characterized by a clay layer with a thickness not exceeding this value.

For 5% damping, the theoretical (Figure 15c,d) and the observed MSA (Figure 18d) are very similar, both in shape and in maximum values, and the two-dimensional model under study can be considered representative for the general geological situation in Mexico City. This is a valuable contribution for micro-zoning purposes, and it permits for each site, where the stratigraphy is reasonably well-known, an estimate of the maximum and average spectral amplification with respect to a bedrock site. An example of the theoretical prediction, based on our results, appropriate for a site similar to the one of station CD (see Fig. 12), is shown in Figure 19a and 19c: the theoretical MSA values are quite satisfactorily compared with the observations made at the station CD in connection with the 1989 event (Figure 19b,d).

Conclusions

The hybrid technique presented in this study makes it possible (1) to study local effects even at large distances (hundreds of kilometers) from the source, (2) to include highly realistic modelling of the source, and (3) of the propagation path. This technique can assist in the interpretation and prediction of ground motion at a given site. It can be applied routinely in (micro-)zonation studies, and provides realistic estimates of ground motion for detailed two-dimensional, anelastic models. The resulting synthetic seismograms can be used to complete existing databases of recorded ground motion. Such databases can then serve to establish estimates of the maximum accelerations, total energies, and spectral amplification of ground motion to be expected at given sites.

The synthetic signals can explain the major characteristics of the observations, even when quite simple source models are assumed. The theoretical computations show that waveforms and frequency content of seismograms are sensitive to small changes in the subsurface topography of the sedimentary basin, the velocity and quality factor of the sediments. What remains constant for different, realistic structural models are the physical processes that occur within sedimentary basins, e.g., the excitation of local surface waves and resonance effects. The frequency content and dispersion characteristics of the waves induced by these processes are clearly related to the depth of the sediments, the steepness and irregularity of the sediment-bedrock interface and the seismic velocities.

To achieve a realistic simulation of seismic ground motion, it is necessary to include source, path and local soil effects, to study both SH and P-SV wave propagation, and to consider anelastic absorption. Following this approach, the reasons for the damage caused by the Michoacan earthquake and the Fucino event can be found not simply in the local site conditions, but also in the effects of the seismic source and of the long-distance propagation path in the crust. The spectral properties of the seismic source and the properties of wave propagation in the crust control the frequency content of the incident wavefield; if a relevant amount of energy is present in the frequency band close to the resonance frequency of the unconsolidated sediments, local surface waves and resonance effects may dominate the horizontal components of motion within the sedimentary basin.

One aspect which is not included in our discussion is the influence of surface topography on ground motion. This approximation can be justified for sites inside sedimentary basins, where topographic features are in general small. However, topography can become important at the edges of sedimentary basins and near outcrops, especially in mountainous regions. The inclusion of the treatment of surface topography is the subject of a forthcoming paper (Fäh and Suhadolc, 1994).

Acknowledgement

We would like to thank Peter Suhadolc and Claudio Iodice for their contribution to this research, ENFA for allowing us the use of the IBM3090E computer at the ENEA INFO BO Computer Center, and the Instituto de Ingeniería of the University UNAM, the Centro de Instrumentación y Registro Sismico of the Fundación Javier Barros Sierra, and the Fundación del grupo Ingenieros Civiles Asosiados for the use of the strong motion data recorded in Mexico City. D.F. has been supported by the Swiss National Science Foundation under Grant Nr. 8220-037189. This study has been made possible by the CNR contracts 91.02692.CT15, 91.02550.PF54 and 92.02867.PF54, and EEC contract EPOC-CT91-0042. This research has been carried out in the framework of the II.P Task Group II.4 contributions to the IDNDR project "Physical Instability of Megacities".

References

AKI, K. and K.L. LARNER (1970): Surface motion of a layered medium having an irregular interface due to incident plane SH waves, *J. Geophys. Res.*, **75**, 933-954.

AMBROSINI, S., S. CASTENETTO, F. CEVOLANI, E. DI LORETO, R. FUNICIELLO, L. LIPERI and D. MOLIN (1986): Risposta sismica dell'area urbana di Roma in occasione del terremoto del Fucino del 13 gennaio 1915, Risultati preliminari. *Mem. Soc. Geol. It.*, **35**, 445-452.

BARD, P.-Y. and M. BOUCHON (1980a): The seismic response of sediment-filled valleys, Part 1: The case of incident SH waves, *Bull. Seism. Soc. Am.*, **70**, 1263-1286.

BARD, P.-Y. and M. BOUCHON (1980b): The seismic response of sediment-filled valleys, Part 2: The case of incident P and SV waves, *Bull. Seism. Soc. Am.*, **70**, 1921-1941.

BARD, P.-Y. and M. BOUCHON (1985): The two-dimensional resonance of sediment-filled valleys, *Bull. Seism. Soc. Am.*, **75**, 519-541.

BARD, P.-Y. and J.-C. GARIEL (1986): The seismic response of two-dimensional sedimentary deposits with large vertical velocity gradients, *Bull. Seism. Soc. Am.*, **76**, 343-366.

BARD, P.-Y., M. CAMPILLO, F.J. CHAVEZ-GARCIA and F.J. SÁNCHEZ-SESMA (1988): The Mexico earthquake of September 19, 1985 - A theoretical investigation of large- and small-scale amplification effects in the Mexico City valley, *Earthquake Spectra*, **4**, 609-633.

BOORE, D.M., K.L. LARNER and K. AKI (1971): Comparison of two independent methods for the solution of wave-scattering problems: Response of a sedimentary basin to vertically incident SH waves, *J. Geophys. Res.*, **76**, 558-569.

CAMPILLO, M., J.-C. GARIEL, K. AKI and F.J. SÁNCHEZ-SESMA (1989): Destructive strong ground motion in Mexico City: Source, path, and site effects during great 1985 Michaocan Earthquake, *Bull. Seism. Soc. Am.*, **79**, 1718-1735.

CNEN-ENEL (1977): Accelerograms from the Friuli, Italy, earthquake of May 6, 1976 and aftershocks: Part 3, uncorrected accelerograms, *Rome, Italy, November 1977.*

DRAKE, L.A. (1980): Love and Rayleigh waves in an irregular soil layer, *Bull. Seism. Soc. Am.*, **70**, 571-582.

ESPINOSA, J.M., G. IBARROLA, O.R. CONTRERAS, V.R. SILVA, L. CAMARILLO and C. PINEDA (1990): Sumario de acelerogramas colectados durante 1990, *Centro de instrumentación y registro sismico, a.c., fundación javier barros sierra, a.c.*

FÄH, D. (1992): A hybrid technique for the estimation of strong ground motion in sedimentary basins, *Ph.D. thesis Nr. 9767, Swiss Federal Institute of Technology, Zurich.*

FÄH, D., P. SUHADOLC and G.F. PANZA (1993a): Variability of seismic ground motion in complex media: the case of a sedimentary basin in the Friuli (Italy) area, *Journal of Applied Geophysics*, **30**, 131-148.

FÄH, D., C. IODICE, P. SUHADOLC and G.F. PANZA (1993b): A new method for the realistic estimation of seismic ground motion in megacities: the case of Rome, *Earthquake Spectra*, **9**, No.4, 643-668.

FÄH, D., P. SUHADOLC, P., ST. MUELLER and G.F. PANZA (1994): A hybrid method for the estimation of ground motion in sedimentary basins; quantitative modelling for Mexico City, *Bull. Seism. Soc. Am.*, *84*, 000-000.

FÄH, D. and P. SUHADOLC (1994): Application of numerical wave-propagation techniques to study local soil effects: The case of Benevento (Italy), Submitted to *Pageoph*.

FEROCI, M., R. FUNICIELLO, F. MARRA and S. SALVI (1990): Evoluzione tettonica e paleogeografica plio-pleistocenica dell'area di Roma, *Il Quaternario*, **3**, 141-158.

FLORSCH, N., D. FÄH, P. SUHADOLC and G.F. PANZA (1991): Complete synthetic seismograms for high-frequency multimode SH-waves, *Pageoph*, 136, 529-560.

FUNICIELLO, R., G. LORIA and S. SALVI (1987): Ricostruzione delle superfici strutturali del sottosuolo della città di Roma, *Atti del 6° Convegno Gruppo Nazionale Geofisica della Terra Solida, CNR, Roma*, 395-415.

GIORGETTI, F. and S. STEFANINI (1989): Vulnerabilità degli acquiferi del campo di Osoppo-Gemona all' inquinamento (Provincia di Udine), *Istituto di Geologia e Paleontologia, Università degli Studi di Trieste*, Pubblicazione n.125.

HASKELL, N.A. (1960): Crustal reflection of plane SH waves, *J. Geophys. Res.*, **65**, 4147-4150.

HASKELL, N.A. (1962): Crustal reflection of plane P and SV waves, *J. Geophys. Res.*, **67**, 4751-4767.

HOUSTON, H. and H. KANAMORI (1986): Source characteristics of the 1985 Michoacan, Mexico earthquake at periods of 1 to 30 seconds, *Geophys. Res. Lett.*, **13**, 597-600.

JACKSON, P.S. (1971): The focusing of earthquakes, *Bull. Seism. Soc. Am.*, **61**, 685-695.

KANAMORI, H., P.C. JENNINGS, S.K. SINGH and L. ASTIZ (1993): Estimation of strong ground motions in Mexico City expected for large earthquakes in the Guerrero seismic gap, *Bull. Seism. Soc. Am.*, **83**, 811-829.

KORN, M. and H. STÖCKL (1982): Reflection and transmission of Love channel waves at coal seam discontinuities computed with a finite difference method, *J. Geophys.*, **50**, 171-176.

LUZON, F., S. AOI, D. FÄH and F.J. SÁNCHEZ-SESMA (1994): Simulation of the seismic response of a 2D sedimentary basin; a comparison between the indirect boundary element method and a hybrid technique. Submitted to *Bull. Seism. Soc. Am.*.

MENA, E., C. CARMONA, R. DELGADO, L. ALCÁNTARA and O. DOMINGUEZ (1986): Catálogo de acelerogramas procesados del sismo del 19 de septiembre de 1985, parte I: Ciudad de México, *Series del Instituto de Ingenieria No. 497, UNAM, México, D. F. México.*

ORDAZ, M. and E. FACCIOLI (1993): Site response analysis in the valley of Mexico: Selection of input motion and extent of nonlinear soil behaviour, *Earthq. Eng. Structural Dynamics*, in press.

PANZA, G.F. (1985): Synthetic seismograms: The Rayleigh waves modal summation, *J. Geophysics*, **58**, 125-145.

RIEDESEL, M.A., T.H. JORDAN, A.F. SHEEHAN and P.G. SILVER (1986): Moment-tensor spectra of the 19 Sept. 85 and 21 Sept. 85 Michaocan, Mexico, earthquakes, *Geophys. Res. Lett.*, **13**, 609-612.

SÁNCHEZ-SESMA, F.J., S. CHÁVEZ-PÉREZ, M. SUÁREZ, M.A. BRAVO and L.E. PÉREZ-ROCHA (1988): The Mexico earthquake of September 19, 1985 - On the seismic response of the Valley of Mexico, *Earthquake Spectra*, **4**, 569-589.

SUAREZ, M., F.J. SÁNCHEZ-SESMA, M.A. BRAVO and J. LERMO (1987): Caracteristicas de los depósitos superficiales del Valle de México, *Memorias VII Congreso Nacional de Ingenieria Sismica, Querétaro, México, November 19-21*, A61-A74.

SUHADOLC, P. and C. CHIARUTTINI (1985): A theoretical study of the dependence of the peak ground acceleration on source and structure parameters, in *strong ground motion seismology*, edited by M.Ö. ERDIK and M.N. TOKSÖZ, *Proceedings of the NATO ASI on Strong Ground Motion Seismology, Ankara, Turkey, 1985*, 143-183.

TRIFUNAC, M.D. (1971): Surface motion of a semi-cylindrical alluvial valley for incident plane SH waves, *Bull. Seism. Soc. Am.*, **61**, 1755-1770.

VENTRIGLIA, U. (1971): La geologia della città di Roma, *Amm. Prov. di Roma, Roma.*

VIRIEUX, J. (1986): P-SV wave propagation in heterogeneous media: Velocity-stress finite-difference method, *Geophysics*, **51**, 889-901.

Layer	Thickness (km)	ρ (g/cm^3)	α (km/s)	β (km/s)	Q_α	Q_β
1	5.0	2.67	4.30	2.53	800	500
2	10.0	2.77	5.70	3.30	800	500
3	15.0	3.09	6.80	4.03	800	500
4	15.0	3.09	7.00	4.10	800	500
5	∞	3.30	8.20	4.82	800	500

Table 1. Numerical parameters for the schematic crustal model describing the path from the source in the Michoacan subduction zone, to Mexico City (Campillo et al., 1989).

FIGURE CAPTIONS

Figure 1. Overview of the Friuli seismic region, showing the presence of the quaternary basin, the ISC epicenter determination of the September 11, Friuli 1976 aftershock ($16^h35^m04^s$), and the position of station Buia. The solid lines indicate the position of the two cross-sections for which 2D modelling has been performed.

Figure 2. Surficial layers of the one-dimensional model, describing the propagation of waves from the source position to the sedimentary basin (Fäh et al., 1993a), and of the 2D models corresponding to cross-sections B and C in Figure 1. Only the part near to the surface is shown, where the 2D models are different from the one-dimensional model.

Figure 3. Acceleration time series for SH and P-SV waves at an array of receivers, for cross-section B shown in Figure 2 (β=0.6 km/s and Q_β=20 for the unconsolidated sediments). All amplitudes are related to a source with a seismic moment of 10^{-7} N m. The signals are normalized to the peak acceleration given in units of cm s^{-2}. The distance to the source for each seismogram is given in units of km. The time scale is shifted by 2 seconds from the origin time (0 s in the figure is really 2 s from the origin time).

Figure 4. Relative peak ground acceleration PGA(2D)/PGA(bedrock) and relative total energy W(2D)/W(bedrock) obtained for cross-section B. The values are shown for four different shear-wave velocities of the sediments (0.5 km/s, 0.6 km/s, 0.7 km/s and 0.8 km/s) and for three different quality factors of the sediments (Q_β=5, Q_β=10, and Q_β=20).

Figure 5. Comparison between (A) the recorded transverse, radial and vertical components of acceleration, and synthetic signals, computed for (B) the cross-section B and (C) the cross-section C. The time-scale is shifted by 2 s from the origin time. The recorded seismograms are aligned to agree with the synthetic signals. All amplitudes of the synthetic signals correspond to a source with a seismic moment of 10^{-7} N m. The synthetic signals are normalized to the same peak acceleration which is given in units of cm s^{-2}.

Figure 6. Damage distribution in Rome caused by the January 13, 1915 Fucino earthquake (after Ambrosini et al., 1986), and thickness of the alluvial sediments (given in meters) (Ventriglia, 1971; Funiciello et al., 1987; Feroci et al., 1990). Three types of damage are distinguished: slight damage (cracking of plaster, the downfall of small pieces of mouldings), intermediate damage (between slight and heavy damage), and heavy damage (deep and diffuse damage of indoor and outdoor walls, downfall of large parts of mouldings and of chimneys). The dashed line indicates the position of the cross section, for which numerical modelling has been performed. The distribution of damage within the area limited by the two dotted lines has been projected on the cross section to construct the histograms, shown in Figure 8.

Figure 7. Approximate epicenter location of the January 13, 1915 earthquake in the Fucino valley (1), and of a hypothetical event (2) located at about 65 km from Rome. The dashed line indicates the cross section along which the numerical modelling has been performed. The source depth is 8 km, the angle between the strike of the fault and the epicenter-station line is 38°, the fault dip 39°, and the rake with respect to the strike 172°. The seismic moment is 10^{19} N m (Fäh et al. 1993b).

Figure 8. A) Total energy W(2D) obtained for the two-dimensional model and the two source positions given in Figure 7, and B) corresponding relative total energy W(2D)/W(bedrock). The results are compared with the histogram of the damage distribution caused by the January 13, 1915 Fucino earthquake. The part of the structure near to the surface, where the 2D model deviates from the 1D bedrock model, is given at the bottom of both parts of the figure.

Figure 9. A) Attenuation of PGA(bedrock), and B) attenuation of W(bedrock) with distance from the seismic source for the one-dimensional layered model (bedrock model).

Figure 10. Fourier-spectra of the signals obtained at 65 km and 85 km from the source for the one-dimensional layered model. The distances correspond to the distance of the eastern margin of the Tiber basin from source 2 and from the Fucino earthquake.

Figure 11. Spectral amplification for the transverse component of motion over the entire cross section, A) for the Fucino event and B) for the hypothetical earthquake. The reference signals are the one obtained for the one-dimensional layered model. At

the bottom of the figure, the geometry of the two-dimensional cross-section is given, while its mechanical parameters are given in Figure 8.

Figure 12. Map of the area of Mexico City showing the locations of strong motion accelerometric stations. The stations represented by large triangles were operating during the 1985 Michoacan event, while the small gray triangles represent the stations which recorded the April 25, 1989 event. The solid line indicates the position of the cross-section, for which the 2D modelling has been performed.

Figure 13. Two-dimensional model of the Chapultepec-Peñon cross-section. Only the part of the structure near to the surface is shown, where the 2D model deviates from the plane-layered structural model (Table 1).

Figure 14. Maximum relative spectral accelerations Sa(2D)/Sa(Ref) (a,c) and velocities Sv(2D)/Sv(Ref) (b,d), for zero damping (a,b) and 5% damping (c,d), obtained with synthetic signals. The results are shown for a single-degree of freedom oscillator for the transverse and the radial component of motion, and for an oscillator with two degrees of freedom for the horizontal ground motion. The synthetic signals are scaled assuming the seismic moment rate spectrum proposed by Kanamori et al. (1993).

Figure 15. Maximum relative spectral velocities Sv(2D)/Sv(Ref), for zero damping (a,b) and 5% damping (c,d), obtained with the synthetic signals, which are scaled by assuming the seismic moment rate spectrum proposed by Kanamori et al. (1993) (a and c), and by assuming a constant, frequency independent, spectrum (b and d).

Figure 16. Observed maximum relative spectral velocities Sv/Sv(TY) for the 1985 Michoacan earthquake, for (a) zero damping and (b) 5% damping. They are determined from the stations SC and CD using TY as reference.

Figure 17. Relative spectral velocities Sv(CD)/Sv(TY), for zero damping (a,b) and 5% damping (c,d). They are determined from the stations CD using TY as reference. Results are shown for the 1985 Michoacan earthquake (a,c) and the April 25, 1989 event (b,d).

Figure 18. Maximum relative spectral velocities Sv/Sv(TY) and Sv/Sv(78) observed during the 1989 event, for zero damping (a,b) and 5% damping (c,d), obtained for all stations shown in Figure 12, using as reference station TY (a,c) and station 78 (b,d), respectively.

Figure 19. Average and maximum relative spectral velocities for zero damping (a), and 5% damping (c), computed with the synthetic signals obtained for the receivers at distances between 408.5 and 410 km from the source. They are compared with the observed relative spectral velocities Sv(CD)/Sv(78) for the 1989 earthquake, for zero damping (b), and 5% damping (d), determined from the station CD using station 78 as reference.

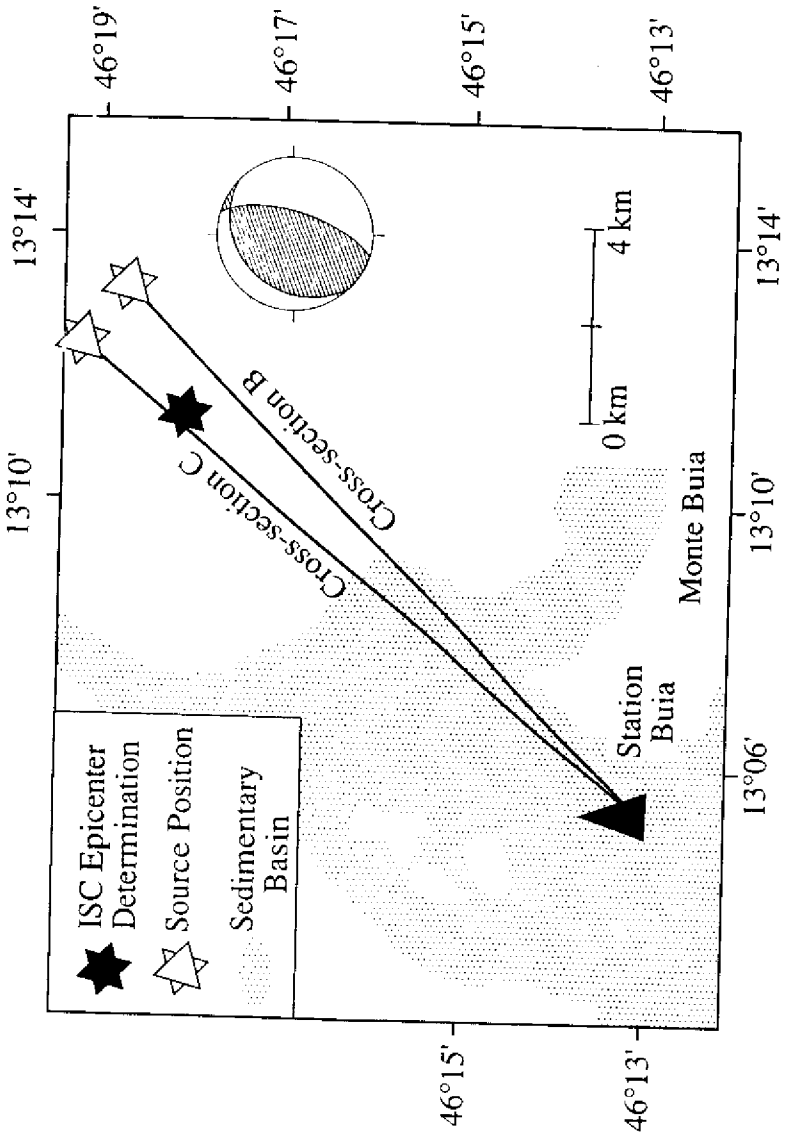
46°19'
46°17'
46°15'
46°13'
13°14'
13°10'
13°06'
4 km
0 km
Cross-section B
Cross-section C
Monte Buia
Station Buia
ISC Epicenter Determination
Source Position
Sedimentary Basin

Fig.1

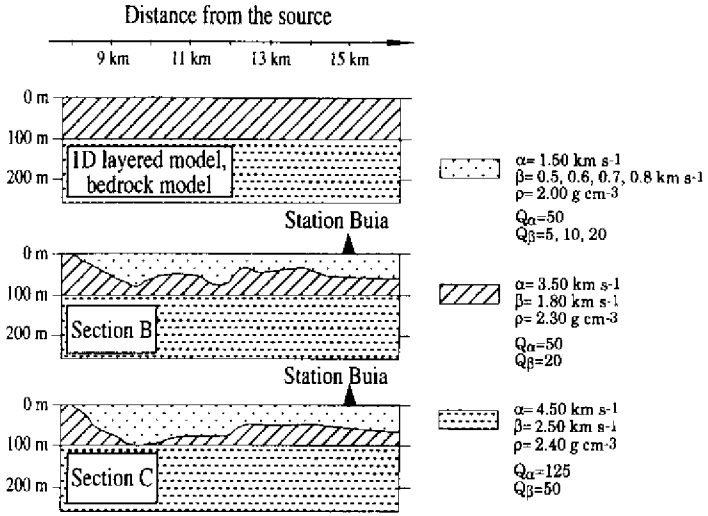
Distance from the source
9 km
11 km
13 km
15 km
0 m
100 m
200 m
1D layered model, bedrock model
Station Buia
Section B
Section C
α= 1.60 km s-1
β= 0.5, 0.6, 0.7, 0.8 km s-1
ρ= 2.00 g cm-3
Qα=50
Qβ=5, 10, 20
α= 3.50 km s-1
β= 1.80 km s-1
ρ= 2.30 g cm-3
Qα=50
Qβ=20
α= 4.50 km s-1
β= 2.50 km s-1
ρ= 2.40 g cm-3
Qα=125
Qβ=50

Fig.2

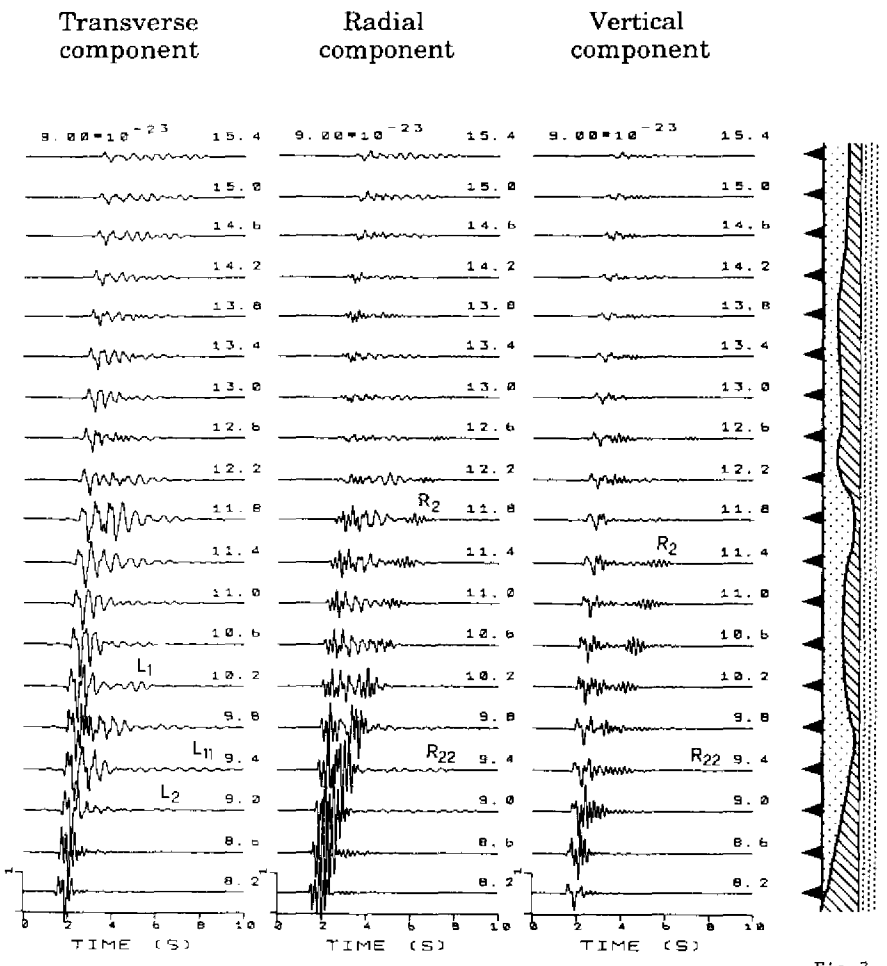
Transverse component
Radial component
Vertical component
TIME (S)
TIME (S)
TIME (S)
L1
Lη
L2
R2
R22

Fig.3

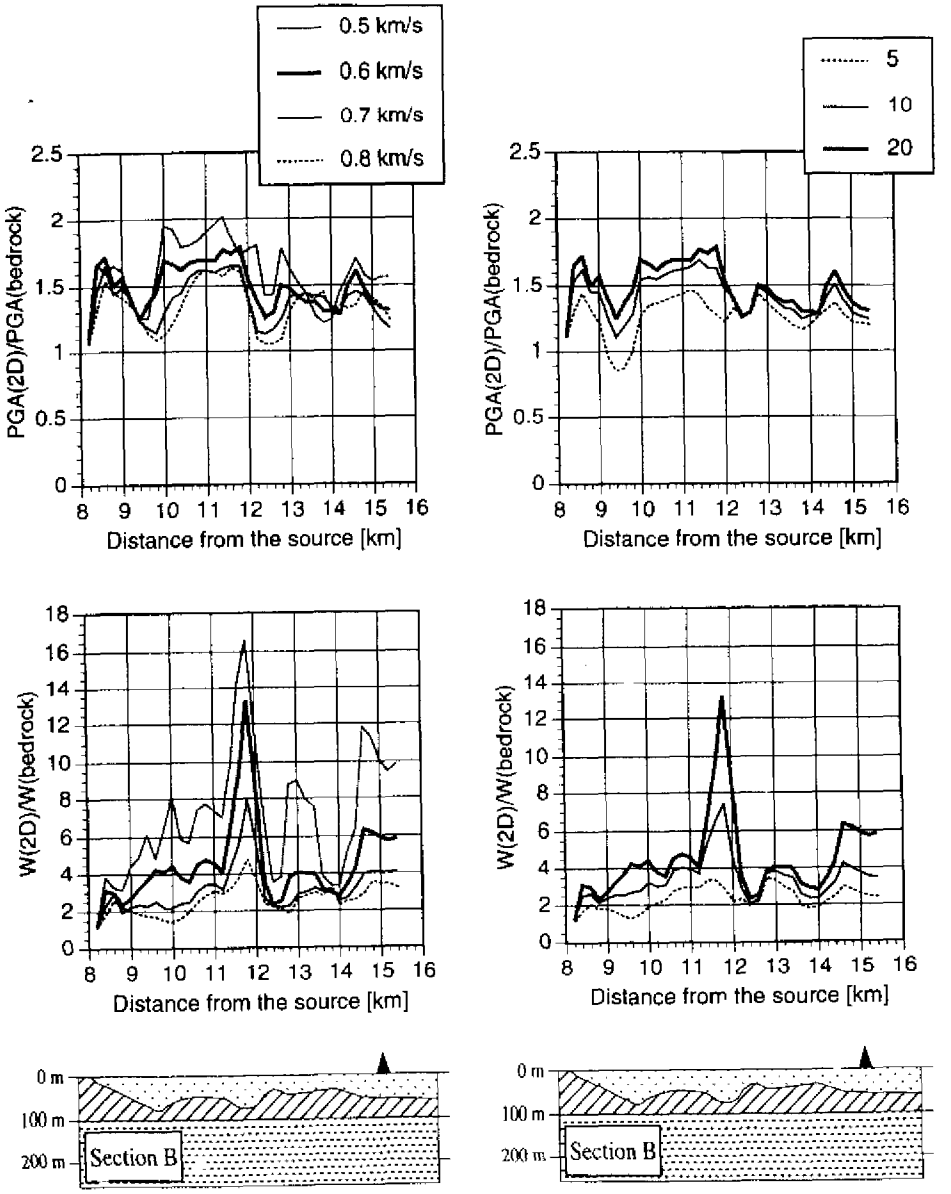
0.5 km/s
0.6 km/s
0.7 km/s
0.8 km/s
5
10
20
PGA(2D)/PGA(bedrock)
W(2D)/W(bedrock)
Distance from the source [km]
0 m
100 m
200 m
Section B

Fig.14

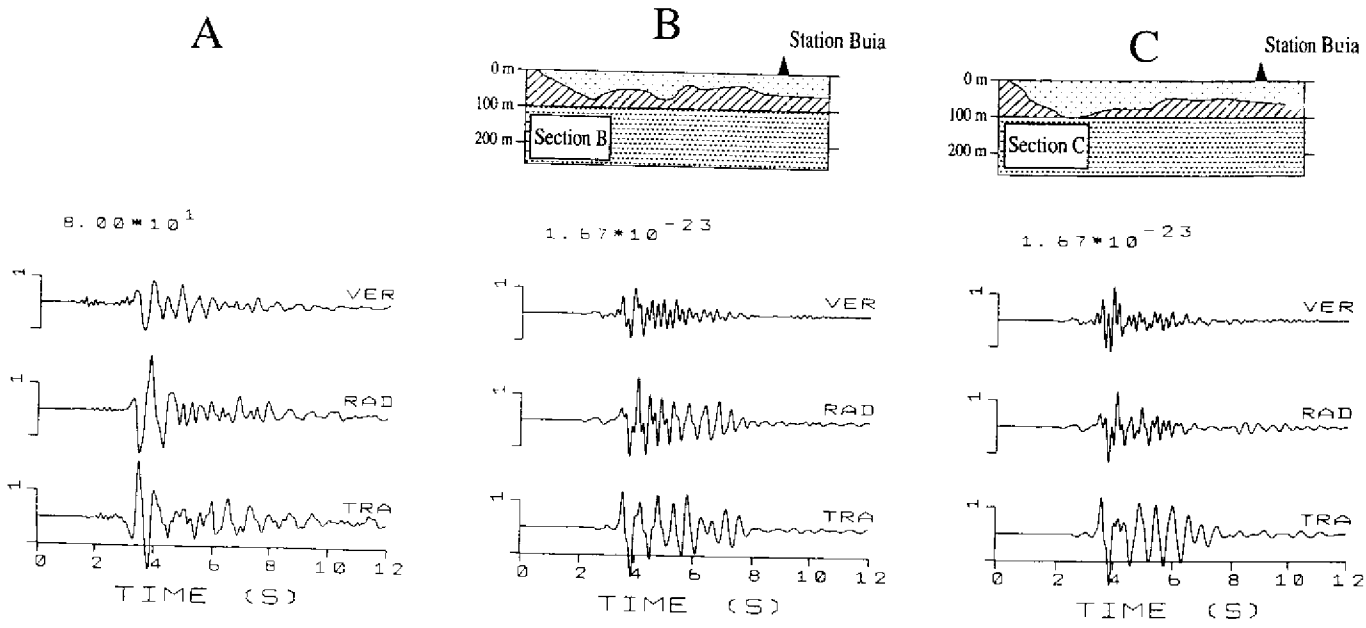

Fig.5

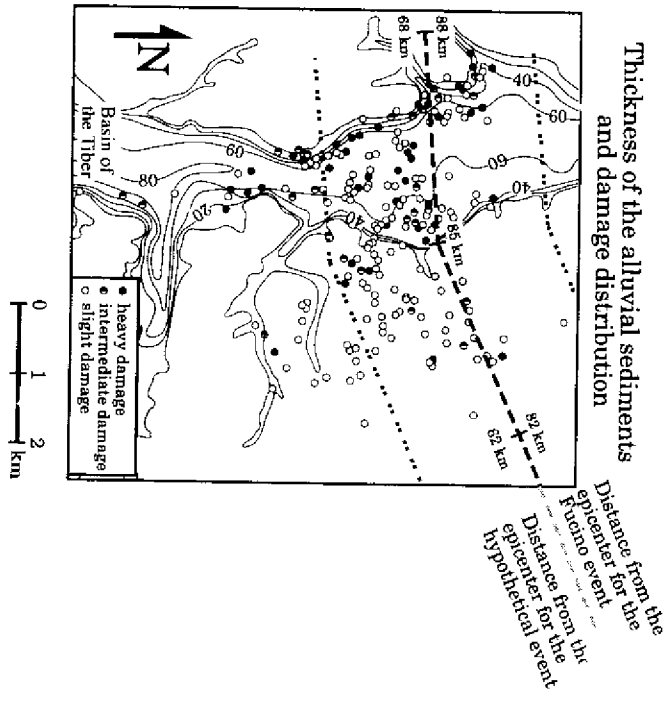

Fig.6

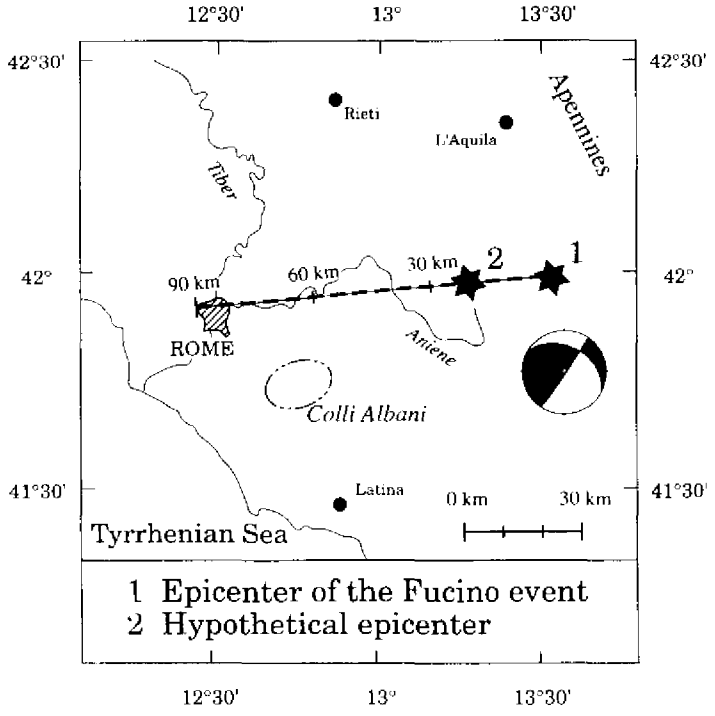
12°30'
13°
13°30'
42°30'
42°
41°30'
Rieti
L'Aquila
Apennines
Tiber
90 km
60 km
30 km
2
1
ROME
Aniene
Colli Albani
Latina
0 km
30 km
Tyrrhenian Sea
1 Epicenter of the Fucino event
2 Hypothetical epicenter

Fig.7

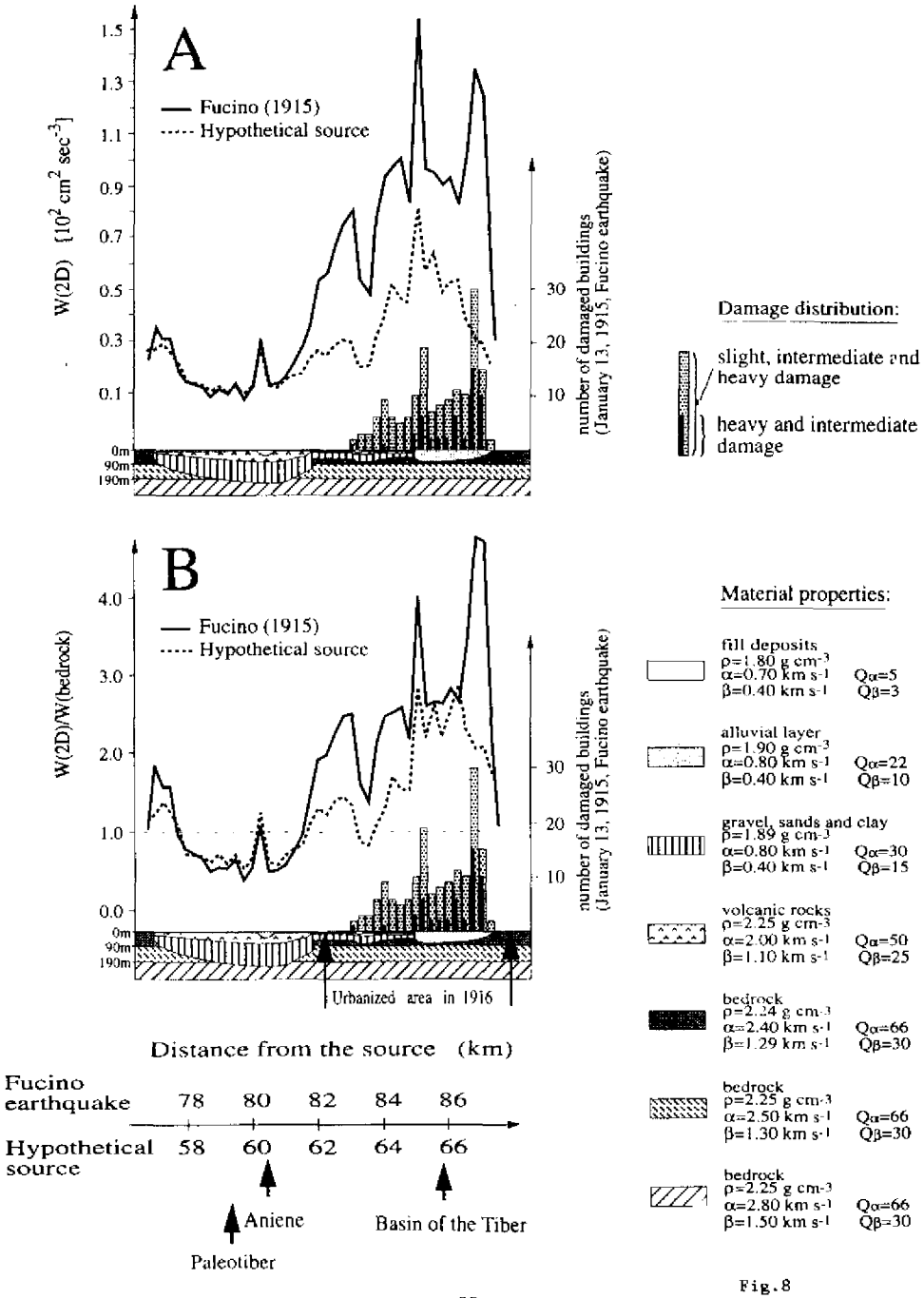
A
Fucino (1915)
Hypothetical source
W(2D) [10² cm² sec⁻³]
number of damaged buildings (January 13, 1915, Fucino earthquake)
0m
90m
190m
B
W(2D)/W(bedrock)
Urbanized area in 1916
Distance from the source (km)
Fucino earthquake
78 80 82 84 86
Hypothetical source
58 60 62 64 66
Aniene
Basin of the Tiber
Paleotiber
Damage distribution:
slight, intermediate and heavy damage
heavy and intermediate damage
Material properties:
fill deposits
ρ=1.80 g cm⁻³
α=0.70 km s⁻¹ Qα=5
β=0.40 km s⁻¹ Qβ=3
alluvial layer
ρ=1.90 g cm⁻³
α=0.80 km s⁻¹ Qα=22
β=0.40 km s⁻¹ Qβ=10
gravel, sands and clay
ρ=1.89 g cm⁻³
α=0.80 km s⁻¹ Qα=30
β=0.40 km s⁻¹ Qβ=15
volcanic rocks
ρ=2.25 g cm⁻³
α=2.00 km s⁻¹ Qα=50
β=1.10 km s⁻¹ Qβ=25
bedrock
ρ=2.24 g cm⁻³
α=2.40 km s⁻¹ Qα=66
β=1.29 km s⁻¹ Qβ=30
bedrock
ρ=2.25 g cm⁻³
α=2.50 km s⁻¹ Qα=66
β=1.30 km s⁻¹ Qβ=30
bedrock
ρ=2.25 g cm⁻³
α=2.80 km s⁻¹ Qα=66
β=1.50 km s⁻¹ Qβ=30

Fig.8

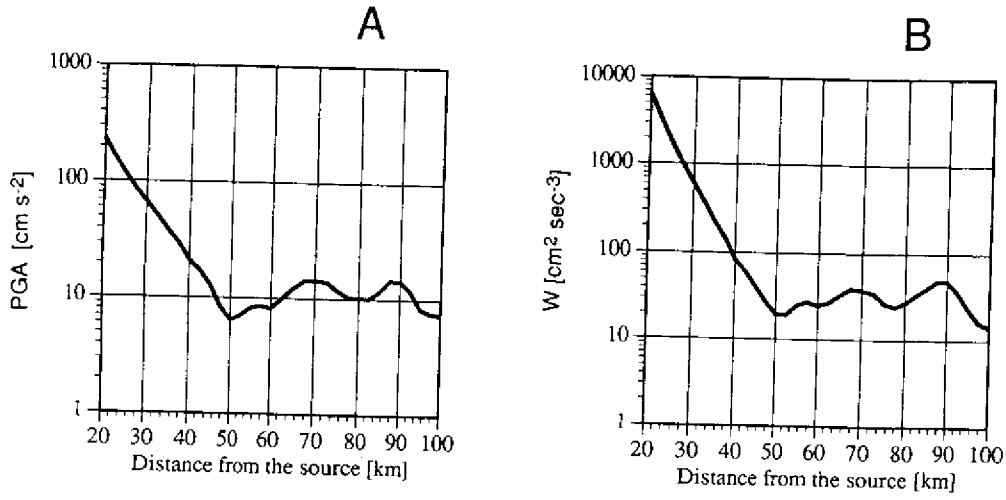
A
PGA [cm s-2]
1000
100
10
1
20 30 40 50 60 70 80 90 100
Distance from the source [km]
B
M [cm2 sec-3]
10000
1000
100
10
1
20 30 40 50 60 70 80 90 100
Distance from the source [km]

Fig.9

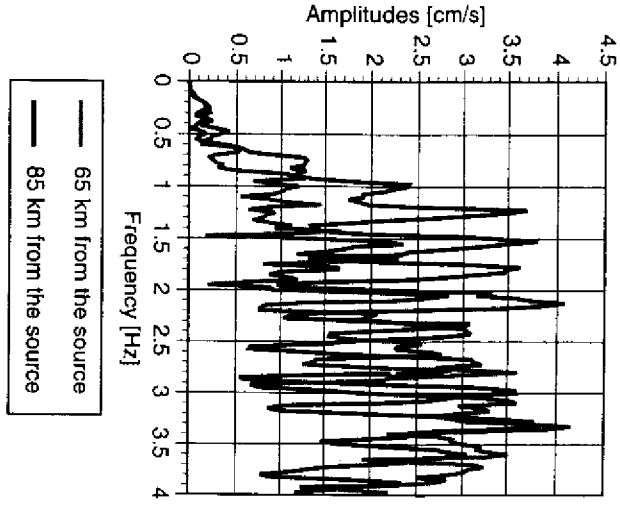
Amplitudes [cm/s]
0 0.5 1 1.5 2 2.5 3 3.5 4 4.5
Frequency [Hz]
0 0.5 1 1.5 2 2.5 3 3.5 4
65 km from the source
85 km from the source

Fig.10

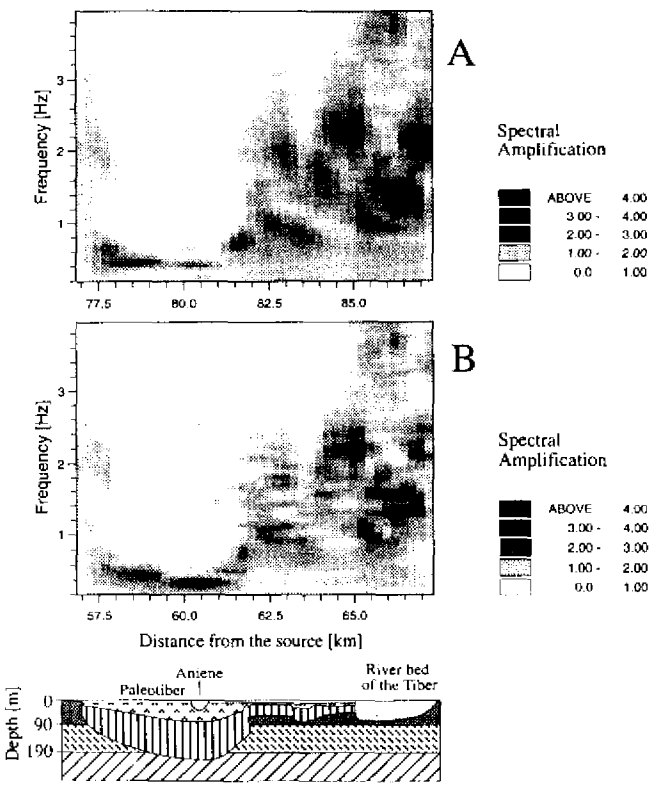
A
B
Frequency [Hz]
Spectral Amplification
ABOVE 4.00
3.00 - 4.00
2.00 - 3.00
1.00 - 2.00
0.0 1.00
77.5 80.0 82.5 85.0
57.5 60.0 62.5 65.0
Distance from the source [km]
Depth [m]
Paleotiber
Aniene
River bed of the Tiber
0
90
190

Fig.11

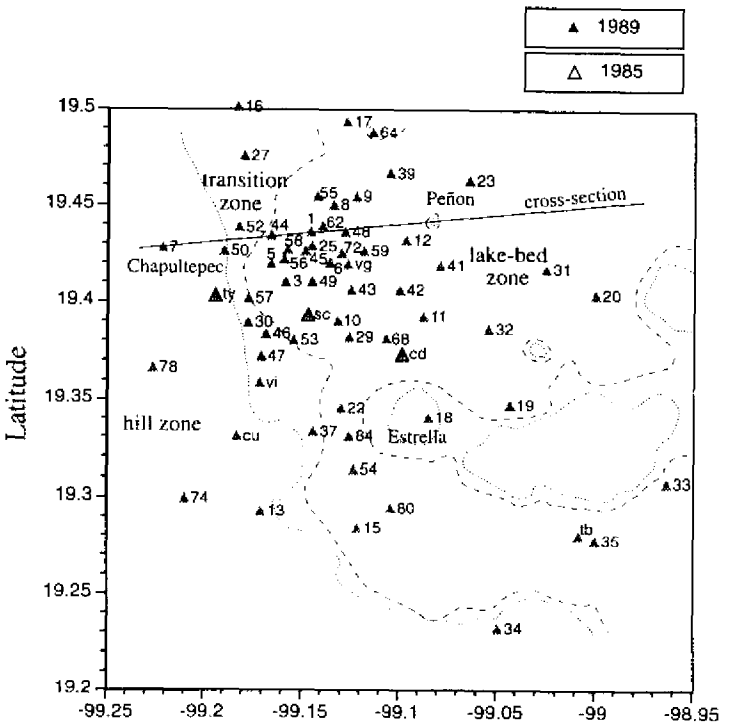
▲ 1989
△ 1985
Latitude
Longitude
19.5
19.45
19.4
19.35
19.3
19.25
19.2
-99.25 -99.2 -99.15 -99.1 -99.05 -99 -98.95
Transition zone
Peñon
cross-section
Chapultepec
lake-bed zone
hill zone
Estrella

Fig.12

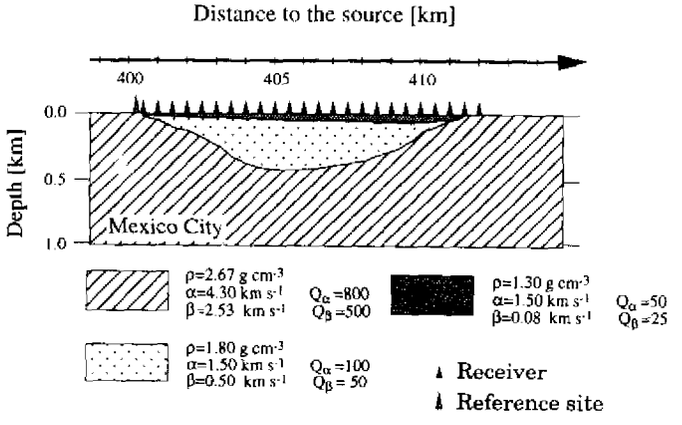
Distance to the source [km]
400
405
410
0.0
0.5
1.0
Depth [km]
Mexico City
ρ=2.67 g cm-3
α=4.30 km s-1
β=2.53 km s-1
Qα=800
Qβ=500
ρ=1.30 g cm-3
α=1.50 km s-1
β=0.08 km s-1
Qα=50
Qβ=25
ρ=1.80 g cm-3
α=1.50 km s-1
β=0.50 km s-1
Qα=100
Qβ=50
Receiver
Reference site

Fig.13

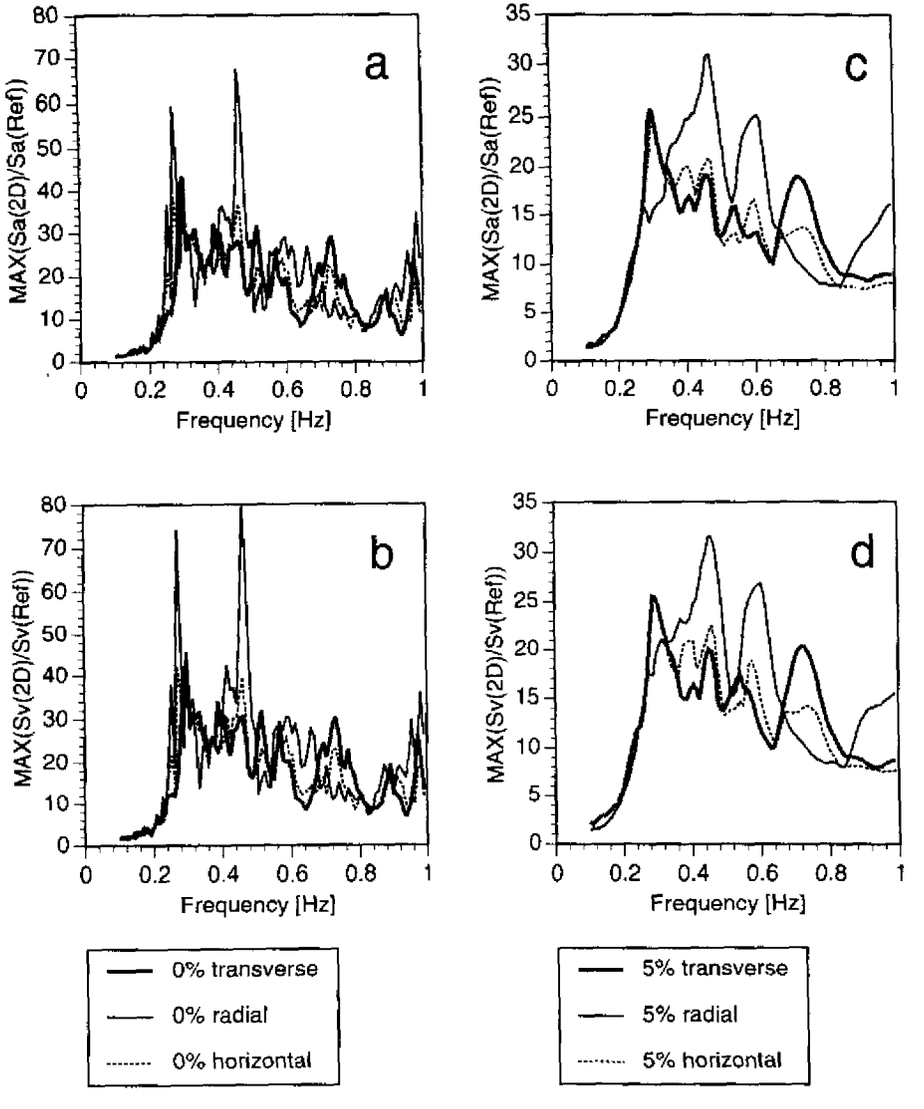
a
b
c
d
MAX(Sa(2D)/Sa(Ref))
MAX(Sv(2D)/Sv(Ref))
Frequency [Hz]
0% transverse
0% radial
0% horizontal
5% transverse
5% radial
5% horizontal

Fig.14

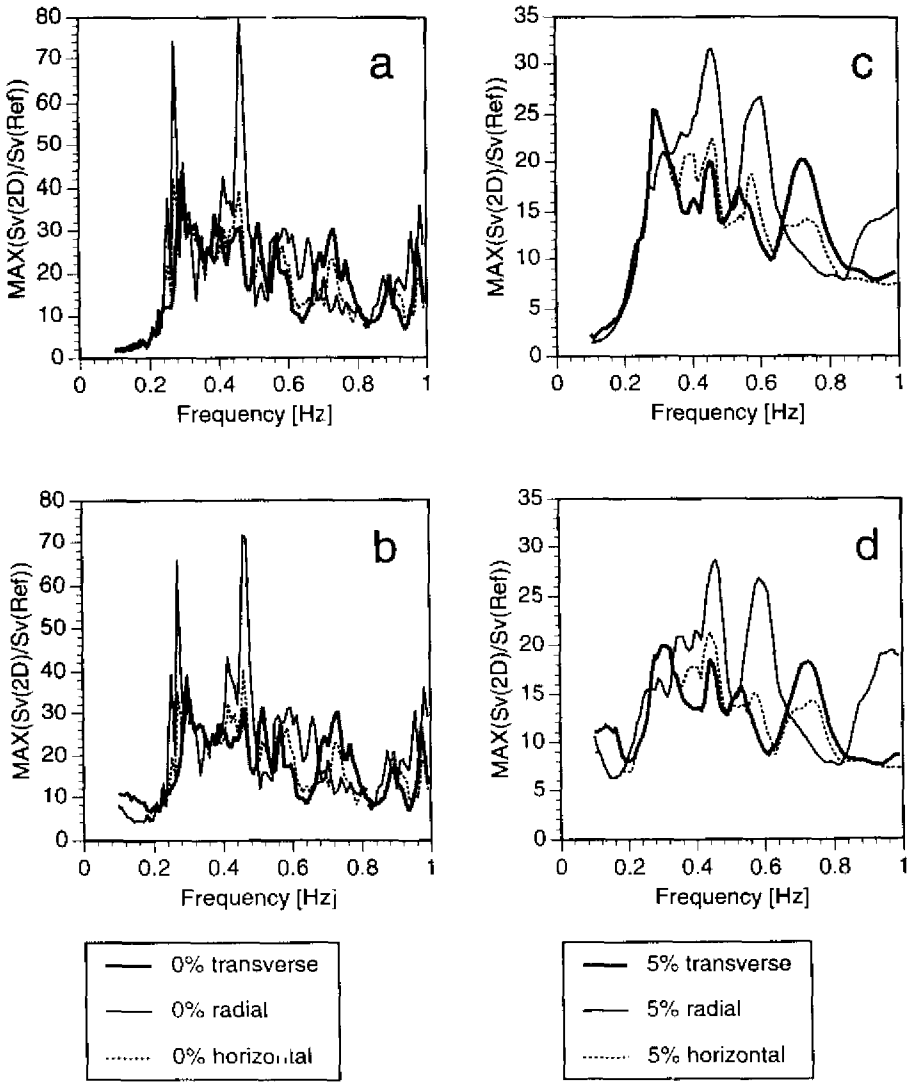
a
c
b
d
MAX(Sv(2D)/Sv(Ref))
Frequency [Hz]
0% transverse
0% radial
0% horizontal
5% transverse
5% radial
5% horizontal

Fig.15

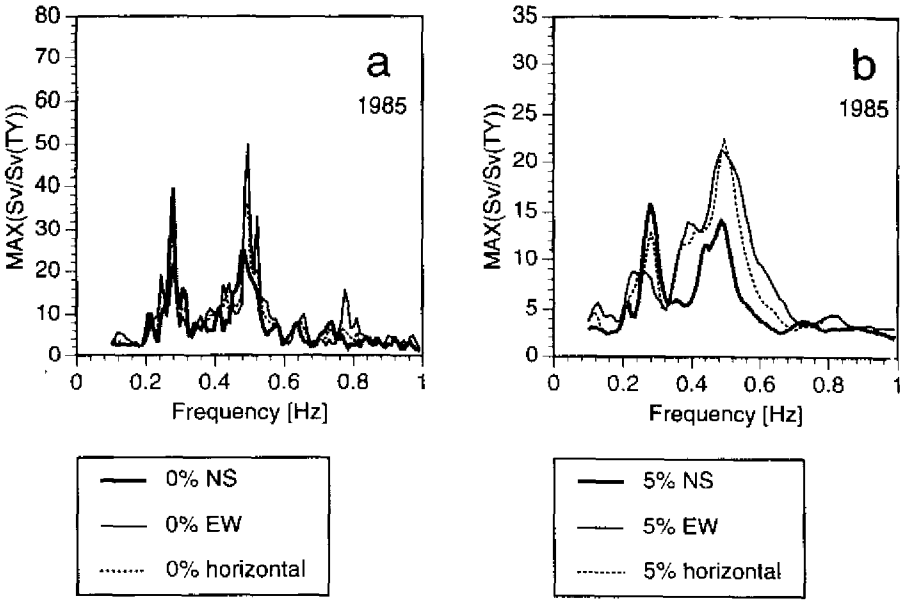
a
1985
b
1985
MAX(Sv/Sv(TY))
Frequency [Hz]
0% NS
0% EW
0% horizontal
5% NS
5% EW
5% horizontal

Fig.16

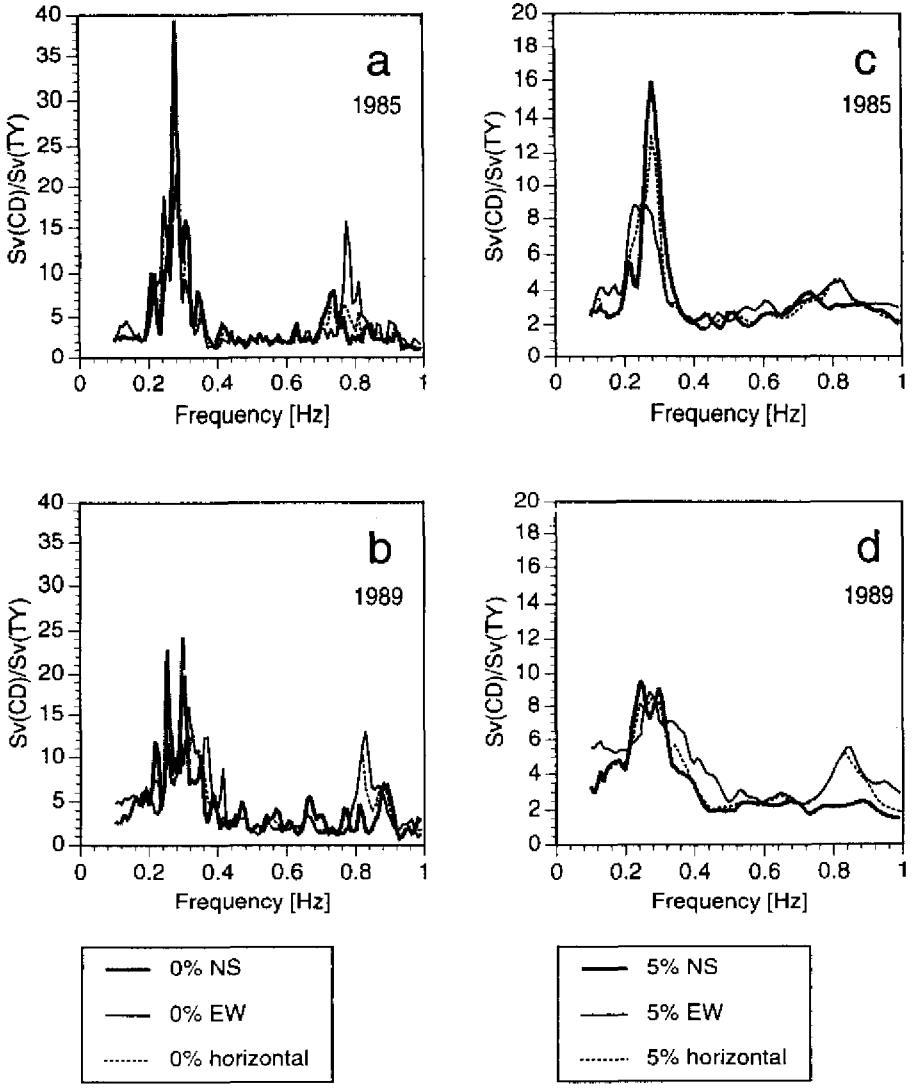
a
1985
c
1985
b
1989
d
1989
Sv(CD)/Sv(TY)
Frequency [Hz]
0% NS
0% EW
0% horizontal
5% NS
5% EW
5% horizontal

Fig.17

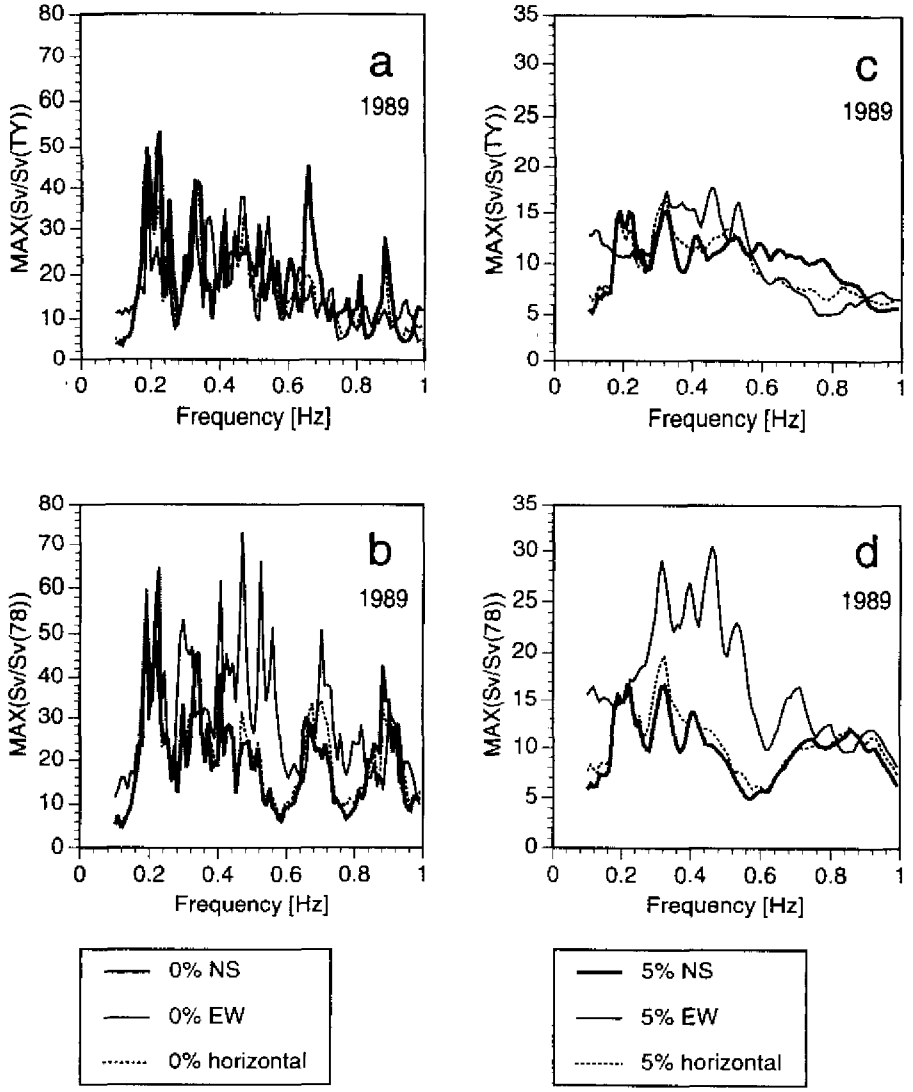
a
1989
c
1989
b
1989
d
1989
MAX(Sv/Sv(TY))
MAX(Sv/Sv(78))
Frequency [Hz]
0% NS
0% EW
0% horizontal
5% NS
5% EW
5% horizontal

Fig.18

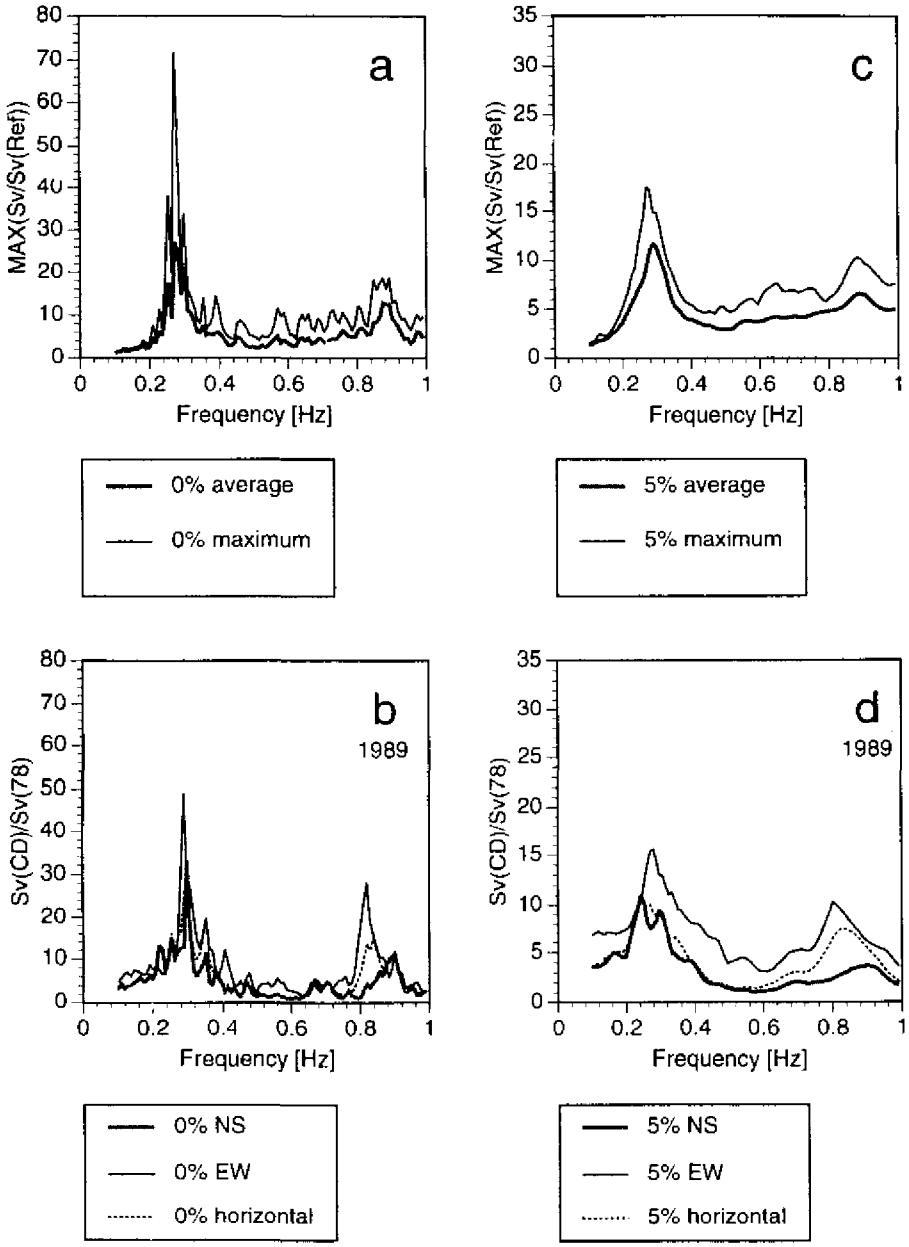
a
MAX(Sv/Sv(Ref))
Frequency [Hz]
0% average
0% maximum
c
MAX(Sv/Sv(Ref))
Frequency [Hz]
5% average
5% maximum
b
1989
Sv(CD)/Sv(78)
Frequency [Hz]
0% NS
0% EW
0% horizontal
d
1989
Sv(CD)/Sv(78)
Frequency [Hz]
5% NS
5% EW
5% horizontal

Fig.19